Morphology Development of Polymeric Microparticles in Aqueous Dispersions. I. Thermodynamic Considerations

DONALD C. SUNDBERG,* ANTHONY P. CASASSA,† JOHN PANTAZOPOULOS,‡ and MARK R. MUSCATO,§
Department of Chemical Engineering, University of New Hampshire, Durham, New Hampshire 03824, and BENGT KRONBERG and JOHAN BERG, *Institute for Surface Chemistry, Stockholm, Sweden*

Synopsis

A thermodynamic analysis of polymer particle morphology highlights the role of interfacial tensions in controlling particle structure. The influence of the surfactant and the nature of the incompatible polymers is seen through their individual and collective effects upon these interfacial tensions. It has been found that by simply changing the type of surfactant used in the emulsion the particle morphology can change from core-shell to hemispherical, in agreement with thermodynamic predictions. Several apparently different morphologies (hemispherical, sandwich, multiple lobes) have been found to coexist at the same time within a single emulsion, suggesting that they may be simply different states of phase separation and not thermodynamically stable, unique morphologies. The thermodynamic analyses are independent of particle size and method of emulsion processing. Experimental evidence shows that the morphology of particles formed via *in situ* polymerization (as in a synthetic latex) is controlled by interfacial tensions in the same manner as those particles formed via solvent evaporation from a solution of an incompatible polymer pair (as in an artificial latex or microencapsulation).

INTRODUCTION

Polymer blends and alloys have emerged as an extremely important material group and increasingly demand the attention of both academic and industrial researchers. These blends range from completely homogeneous ones[1] to completely phase-separated ones. The morphological configurations that the latter possess are critically important in determining the physical property spectrum of the material.[2] Such blends display enhanced properties over their single-phase counterparts when the size and shape of the microdomains and the interfacial region are properly controlled.

Many important polymer blends are, or can be, produced in the form of microscopic particles dispersed in a low viscosity liquid, typically water. Synthetic and artificial latices and microencapsulated particles are common examples of multiphase polymeric particles for which morphology is a prime con-

* To whom correspondence should be addressed.
† Present address: Janco P/C, Inc., Dover, NH 03820.
‡ Present address: Morton Thiokol, Inc., Ventron Division, Danvers, MA 01923.
§ Present address: Waters Chromatography Division, Millipore Corporation, Taunton, MA 02780.

Journal of Applied Polymer Science, Vol. 41, 1425–1442 (1990)
 CCC 0021-8995/90/7-81425-18$04.00

tributor to the performance characteristics of the material. As compared to bulk-phase polymer blends, these particles have the addition of a water/particle interface that is nearly always partially covered with a surfactant to achieve colloidal stability. We have recently reported on the influence of the nature of that water/particle interface on the resultant morphology of polymer encapsulated oil droplets.[3,4]

A review of the literature reveals that a great variety of different particle morphologies have been reported. These include the familiar core-shell ([5–8] among others), "inverted" core-shell,[5,9,10] sandwich structures,[5] hemispheres,[5,11] and "confetti-like," "raspberry-like," and "void" particles.[12] It is also evident from viewing photomicrographs of commercial resins such as acrylonitrile–butadiene–styrene (ABS) that combinations of some of the above morphologies also exist. Given that the morphologies reported in the above references were derived from a wide variety of materials and process conditions, it would appear that the development of a general understanding of the factors that control particle morphology would be of great benefit. Although this is likely to be a rather complex matter, the purpose of this article is to describe a rather straightforward approach that offers substantial insight into the basic factors controlling particle morphology.

THERMODYNAMIC CONSIDERATIONS

It is clear that the development of the final morphology in polymer microparticles involves the movement, or diffusion, of at least two molecular species under the influence of some driving force to attain the phase-separated arrangement. Although the ease of movement will certainly be related to the viscosity of the phases, that issue will be put aside for the moment to concentrate upon the driving force. By considering the following hypothetical pathway for morphology development, the driving force will readily be seen as the Gibbs free energy change of the process. The initial state is considered to be that of a particle of pure polymer 1 suspended in water containing some surfactant, and a bulk phase of pure polymer 2 (phase incompatible with polymer 1), completely separated from each other. The final state is that of one of the morphologies shown in Figure 1 at the same temperature and pressure as the completely phase-separated initial state. Since no phase changes, mixing or demixing are involved, the only contribution to the free energy change is that of the creation of new interfaces. Those interfaces are polymer 1/water, polymer 2/water, and polymer 1/polymer 2. It needs to be emphasized at this point that the practical need for a stabilizing agent may greatly affect the interfacial tension at the water/particle interface. Accordingly, the total free energy change for any of the configurations shown in Figure 1, viewed here as the driving force for morphology development, can be expressed as

$$\Delta G = \sum_i \gamma_i A_i - \gamma_{\mathrm{plw}} A'_o \tag{1}$$

where γ_i is the interfacial tension of the ith interface and A_i is the corresponding interfacial area. Thus, γ_{plw} is the interfacial tension of the original polymer 1

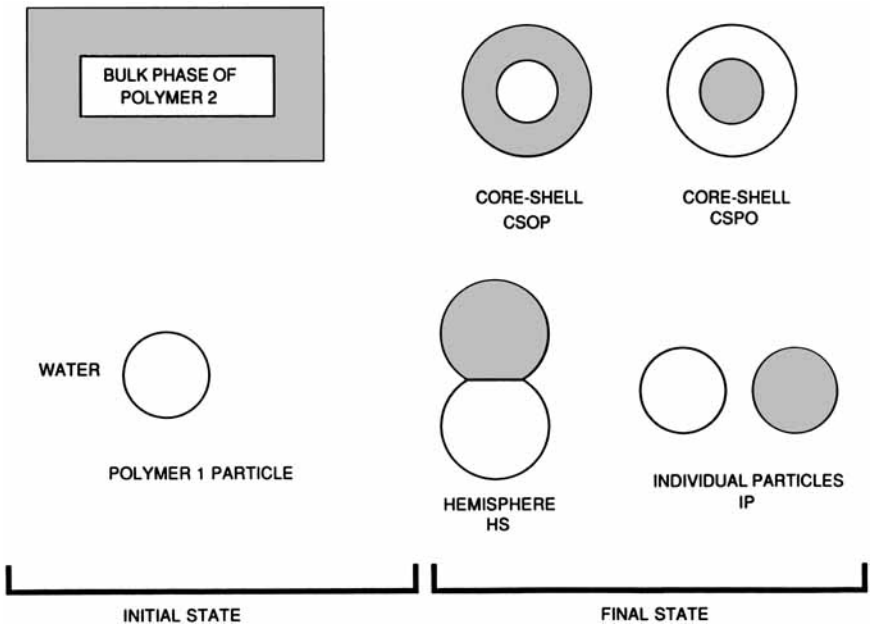

Fig. 1. Initial and final states for morphology development.

particle suspended in water (containing surfactant, if present) and A'_o its interfacial area.

Each of the morphologies depicted in Figure 1 will have different combinations of $\gamma_i A_i$ due only to their geometry. The morphology of the thermodynamically preferred system will be that which has the minimum interfacial free energy. This makes the analysis quite straightforward and results in a practical application if all of the γ_i can be measured independently of the morphology development process. The first case to be treated is that of the core-shell arrangement with polymer 2 encapsulating polymer 1. For ease of discussion and simplicity of notation, this morphology is designated as CSOP [*c*ore-*s*hell, *o*riginal polymer (1) as core, secondary *p*olymer (2) as shell]. The free energy change for the formation of this morphology is

$$(\Delta G)_{\text{CSOP}} = \gamma_{\text{op}} 4\Pi R_o^2 + \gamma_{\text{pw}} 4\Pi R_p^2 - \gamma_{\text{ow}} 4\Pi (R'_o)^2 \qquad (2)$$

where the interfacial tensions are those between the two polymers, γ_{op}, polymer 2 and water, γ_{pw}, and polymer 1 and water, γ_{ow}. R'_o is the radius of the original polymer 1 particle, R_o is that of the core of the CSOP arrangement, and R_p is the outer radius of the CSOP particle. In this particular case, $R_o = R'_o$. It is useful to reduce $(\Delta G)_{\text{CSOP}}$ in eq. (2) by A'_o and to describe the free energy change per unit surface area of the original polymer 1 particle as

$$(\Delta\gamma)_{\text{CSOP}} = \frac{(\Delta G)_{\text{CSOP}}}{A'_o} \qquad (3)$$

This is denoted as $\Delta\gamma$ because the reduced free energy has the same units as

interfacial tension, mN/m. It is further advantageous to work in terms of the volume fraction ϕ_p, of polymer 2 in the final particle, which is described as

$$\phi_p = V_p/(V_p + V_o) = 1 - (R_o/R_p)^3 \tag{4}$$

where V_p and V_o are the volumes of polymer 2 and polymer 1, respectively. Combining eqs. (2), (3), and (4)

$$(\Delta\gamma)_{\text{CSOP}} = \gamma_{\text{op}} + \gamma_{\text{pw}}(1 - \phi_p)^{-2/3} - \gamma_{\text{ow}} \tag{5}$$

For the case in which polymer 2 becomes the core and polymer 1 the shell, the particle is designated CSPO. Such an arrangement may be called inverted core-shell. In a manner similar to that shown above,

$$(\Delta G)_{\text{CSPO}} = \gamma_{\text{op}} 4\Pi R_p^2 + \gamma_{\text{ow}} 4\Pi R_o^2 - \gamma_{\text{ow}} 4\Pi (R_o')^2 \tag{6}$$

Note that in this case $R_o \neq R_o'$ and ϕ_p is written as

$$\phi_p = V_p/(V_p + V_o) = \frac{(R_p/R_o')^3}{[1 + (R_p/R_o')^3]} \tag{7}$$

Hence, the reduced free energy change is

$$(\Delta\gamma)_{\text{CSPO}} = \gamma_{\text{ow}}[(1 - \phi_p)^{-2/3} - 1] + \gamma_{\text{op}}[\phi_p/(1 - \phi_p)]^{2/3} \tag{8}$$

The simplest case is that of individual particles, IP, and although such a morphology might never be achieved in practice, it does serve as a useful reference point. Here

$$(\Delta G)_{\text{IP}} = \gamma_{\text{pw}} 4\Pi R_p^2 \tag{9}$$

$$\phi_p = V_p/(V_p + V_o) = (R_p/R_o')^3/[1 + (R_p/R_o')^3] \tag{10}$$

and

$$(\Delta\gamma)_{\text{IP}} = \gamma_{\text{pw}}[\phi_p/(1 - \phi_p)]^{2/3} \tag{11}$$

The case for the hemispherical morphology, HS, is more complicated in a geometrical sense and an approximate (but nearly accurate) analysis is useful at this point. Figure 2 represents this approximation and defines the new parameters h and R which are clearly related to the volume fraction of polymer 2. For this geometry

$$(\Delta G)_{\text{HS}} = \gamma_{\text{pw}} 2\Pi R h + \gamma_{\text{ow}} 2\Pi R(2R - h) + \gamma_{\text{op}} \Pi h(2R - h) - \gamma_{\text{ow}} 4\Pi (R_o')^2 \tag{12}$$

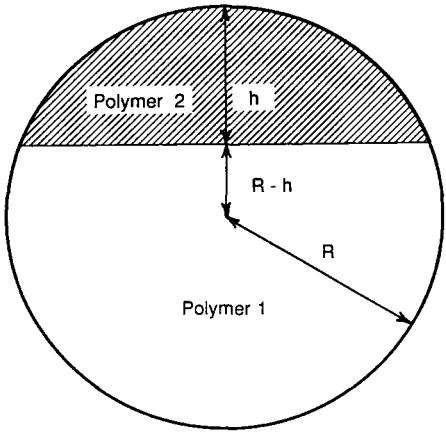

Fig. 2. Particle morphology for approximate hemispherical analysis.

Here

$$\phi_p = [R^3 - (R'_o)^3]/R^3 = 1 - (R'_o/R)^3 \tag{13}$$

After some algebra

$$(\Delta\gamma)_{HS} = (1 - \phi_p)^{-2/3}\{\gamma_{pw}(h/2R) + \gamma_{ow}[1 - (h/2R) - (1 - \phi_p)^{2/3}] + \gamma_{op}(h/2R)[1 - (h/2R)]\} \tag{14}$$

where

$$4\phi_p = 6(h/2R) - 1 + [1 - 2(h/2R)]^3 \tag{15}$$

Computation of $(\Delta\gamma)_{HS}$ via eq. (14) must be done by using eq. (15) to obtain the value of $(h/2R)$ from the chosen value of ϕ_p.

A more accurate analysis of the free energy change for the hemispherical morphology is presented in the Appendix. The analysis involves a trial and error solution for the interfacial energy at any given volume fraction of polymer 2, in contrast to the direct approach using eqs. (14) and (15). The $(\Delta\gamma)_{HS}$ curves plotted in the figures shown in this paper are those determined from the more accurate approach shown in the Appendix. Using eqs. (14) and (15) to obtain $(\Delta\gamma)_{HS}$ vs. ϕ_p, the reader can compare the results obtained from both approaches if it is desired.

It is of significant interest to look at the limiting behavior of the $(\Delta\gamma)$ equations as the volume fraction of polymer 2 approaches zero. Such a situation is approximated in practice when it is desired to produce a core-shell morphology (CSOP) with an extremely thin shell of the second polymer. Taking the limit of eqs. (5), (8), (11), and (14) as ϕ_p goes to zero results in

$$\lim_{\phi_p \to 0} (\Delta\gamma)_{CSOP} = \gamma_{op} + \gamma_{pw} - \gamma_{ow} \tag{16}$$

$$\lim_{\phi_p \to 0} (\Delta\gamma)_{CSPO} = \lim_{\phi_p \to 0} (\Delta\gamma)_{IP} = \lim_{\phi_p \to 0} (\Delta\gamma)_{HS} = 0 \tag{17}$$

Equation (16) is the well-known condition for spreading, applied in this case to the spreading of polymer 2 over the surface of polymer 1. When $\gamma_{ow} > (\gamma_{op} + \gamma_{pw})$, then a core-shell particle would be favored over any of the other morphologies. When the reverse is true, one of the other morphologies would be favored. These results are only strictly true at $\phi_p = 0$ and eqs. (5), (8), (11), and (14) must be used to determine the preferred morphology at higher volume fractions. Results for a number of interesting conditions (i.e., various values of γ_{op}, γ_{ow}, and γ_{pw}) will be described later in this paper.

A similar, but less complete, analysis was presented some time ago by Torza and Mason (13). They studied the phase behavior of low viscosity, immiscible organic liquids dispersed in an aqueous phase as the drops were subjected to varying shear and electric fields. Their photomicrographs clearly showed the existence of core-shell and hemispherical morphologies, the occurrence of which depended upon the various interfacial tensions. They defined the spreading coefficient, S_i, which is written as

$$S_i = \gamma_{jk} - (\gamma_{ij} - \gamma_{ik}) \tag{18}$$

for the premise that $\gamma_{12} > \gamma_{23}$, $S_1 < 0$. For this case Torza and Mason showed that for $S_2 < 0$ *and* $S_3 > 0$ the core shell morphology was preferred. On the other hand, for $S_2 < 0$ *and* $S_3 < 0$ the hemispherical morphology was preferred. The subscripts in eq. (18) were assigned the physical definition as follows: 1 for the first organic liquid, 2 for the water, and 3 for the second organic liquid. Thus, γ_{12} represented the interfacial tension between the first organic liquid and water, γ_{13} that between the two organic liquids, etc.

Torza and Mason applied eq. (18) and the subsequent inequalities to a variety of liquid dispersions and found agreement between predictions and experimental results. It should be noted here that both low-viscosity liquids would be able to diffuse rapidly and to assume the lowest interfacial energy morphology within the time frame of the experiment. In contrast, if one worked with two high molecular weight polymers the diffusional resistance may be such that the equilibrium morphology might not be realized during the experiment even though the driving force continues to be present. Thus, Torza and Mason's work with low-viscosity fluids was a good way to test the correctness of the thermodynamic analysis. The application of interfacial thermodynamics to systems containing polymers is the focus of the present paper.

EXPERIMENTAL

The experimental results described in this communication were derived from both reactive processing and physical processing techniques. The reactive processing involved the polymerization of methyl methacrylate (MMA) in the presence of preformed particles, while the physical processing involved the evaporation of a solvent from an initially homogeneous phase particle, resulting in phase separation within the particle. All particles were dispersed within an aqueous phase and stabilized by a variety of surfactants. The triangular diagram shown in Figure 3 describes the different paths followed by the two processes mentioned above. The physical processing method, path A, is in essence that

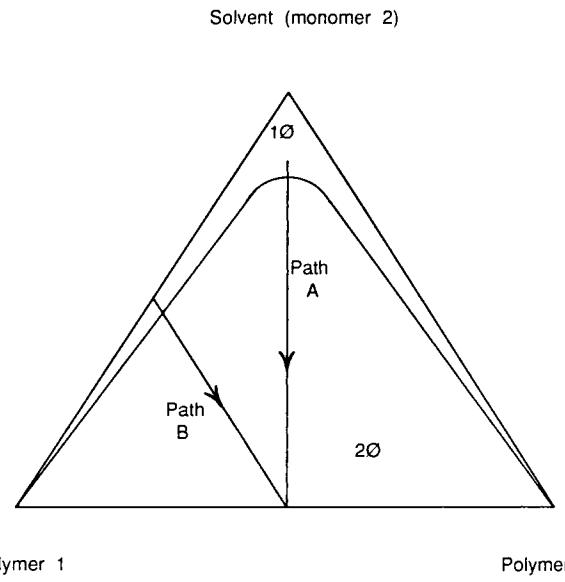

Fig. 3. Process pathways for morphology development. 1 ϕ represents single-phase region; 2 ϕ represents two-phase region.

of preparing an artificial latex and is the physical analogy of synthetic latex production via chemical reaction, path B.

The first step in our experimental program has been to study morphology development in systems for which the diffusional resistance to phase separation within the particle is significantly greater than that encountered in the work of Torza and Mason,[13] but significantly less than that corresponding to incompatible blends of high molecular weight polymer pairs. As such, we have chosen to work with a high molecular weight polymer and an incompatible hydrocarbon oil. The polymer chosen for this study was poly(methyl methacrylate) (PMMA) and the oil was either *n*-decane or mineral oil.

The preparation of two-phase microparticles via the chemical processing route using *n*-decane as the oil has been described in detail elsewhere.[4] Briefly, an organic peroxide initiator was dissolved in the *n*-decane and emulsified in water containing a surfactant. The MMA monomer was then added to the water phase, the resultant mixture heated, and polymerization took place.

The physical processing route utilized mineral oil (Diamond Drug, Inc., extra heavy grade) or *n*-decane (J. T. Baker, practical grade) and preformed PMMA (Eastman Kodak Co., practical grade) dissolved together in methylene chloride (J. T. Baker, HPLC grade). The oil and polymer each constituted 6.6 wt % of these three component solutions, which were then emulsified (Biospec Products Biohomogenizer) in water containing a surfactant. Samples of these emulsions were then placed on microscope slides and photomicrographs were taken to document morphology development as the solvent diffused out of the particles, through the water, and evaporated at the edge of the microscope slide.

Interfacial tensions between the oils and the water (containing surfactant) were determined by the du Nuoy ring method (at very slow rates of ring movement) or by the drop-volume technique.[14] The latter technique is very simple

to perform and is quite reproducible as long as the liquid viscosities are not too high. The interfacial tensions between the water (with surfactant) and the PMMA were determined by measuring the contact angle of an aqueous drop on a PMMA-coated glass slide. The PMMA used to coat the glass slide was the same as that used to perform the morphology experiments. The static contact angle was measured. In addition, it was necessary to determine the surface tension of the aqueous phase with a du Nuoy ring and to obtain a value for the surface tension of the PMMA. The latter was taken to be 41.1 mN/m at 20°C after Wu.[15] These values were used in Young's equation

$$\sigma_p = \gamma_{pw} + \sigma_w \cos \Theta \tag{19}$$

to determine γ_{pw}. In eq. (19), σ_p is the polymer surface tension, σ_w is the aqueous (with surfactant) surface tension, and Θ is the contact angle.

The surfactants used in these studies represented two ends of the spectrum of surface activity. Sodium lauryl sulfate (SLS) (Aldrich Chemical Co.) was used to achieve low interfacial tensions of the organic phases against water, and a natural pectin (Mexpectin XSS100, Grinsted Products, Denmark) was used to achieve much higher interfacial tensions, all the while maintaining adequate mechanical stability of the emulsion. The surfactants were dissolved at 0.5 wt % in vacuum boiled, deionized water for emulsion preparation.

RESULTS AND DISCUSSION

The calculation of the reduced surface energy of each of the four equilibrium morphologies of interest can be done using eqs. (5), (8), (11), (14), and (15). As noted earlier, we have used eq. (A8) instead of eqs. (14) and (15) to gain a little more accuracy for the hemispherical morphology. These computations have been carried out as a function of the weight fraction of PMMA, and required numerical values for γ_{ow}, γ_{pw} (via Θ), and γ_{op}. The values for these

TABLE I
Measured Interfacial Tensions and Contact Angles

	Θ (°)	γ_{ow}, γ_{pw} (mN/m)
Mineral oil/water		
Pure water	—	64.4
0.5% MXP aqueous solution	—	55.7
0.5% SLS aqueous solution	—	13.2
n-Decane/water		
Pure water	—	49.9
0.5% MXP aqueous solution	—	44.1
0.5% SLS aqueous solution	—	6.7
PMMA/water		
Pure water	70.5	17.1
0.5% MXP aqueous solution	67.5	15.9
0.5% SLS aqueous solution	37.5	13.3

interfacial tensions are shown in Tables I and II. Those for γ_{ow}, Θ, and γ_{pw} were from experimental measurements as described earlier, while the γ_{op} values were predicted by use of the harmonic mean eq. (15),

$$\gamma_{op} = \sigma_o + \sigma_p - 4[\sigma_o^d\sigma_p^d/(\sigma_o^d + \sigma_p^d) + \sigma_o^p\sigma_p^p/(\sigma_o^p + \sigma_p^p)] \quad (20)$$

In the above equation, σ_o^d and σ_p^d are the dispersive components of the *surface* tensions of the oil and polymer, while σ_o^p and σ_p^p are the respective polar components. These two components are related as

$$\sigma_i = \sigma_i^d + \sigma_i^p \quad (21)$$

and the fractional polarity, X_i^p, is defined as

$$X_i^p = \sigma_i^p/\sigma_i \quad (22)$$

γ_{op} was predicted rather than experimentally measured by utilizing the contact angle between an oil droplet and a polymer film because γ_{op} is so low that the oil nearly completely wets the polymer. This results in a contact angle so low that it would not be measured with much accuracy.

Figures 4 and 5 show the results of the computations for the reduced surface energies ($\Delta\gamma$) of the PMMA/*n*-decane system with Mexpectin XSS100 (MXP) and SLS as surfactants, respectively. For the use of MXP, Figure 4 shows that over the entire range of weight fractions of PMMA in the final particle the core-shell morphology clearly has the lowest computed interfacial energy and is thus the preferred equilibrium morphology. When the surfactant is changed to SLS, the core-shell morphology is computed to have the highest interfacial energy and thus one of the other morphologies should be preferred. Using the spreading coefficient analysis of Torza and Mason[13] for this case one would not be able to distinguish between the alternate morphologies since the analysis only applies at $\phi_p = 0$. However, the reduced surface energy analysis detailed in the present paper clearly shows that the hemisphere morphology is preferred when SLS is used in the PMMA/*n*-decane system.

TABLE II
Computed Interfacial Tensions

	PMMA	Mineral oil	*n*-Decane
σ, mN/m	41.1[a]	29.6[b]	23.9[b]
σ^d, mN/m	29.6[a]	29.6	23.9
σ^p, mN/m	11.5[a]	0.0	0.0
X^p	0.28[a]	0.0[c]	0.0[c]
γ_{op}, mN/m	—	11.5[d]	12.1[d]

[a] After Wu.[15]
[b] Measured.
[c] Via solubility parameters.
[d] γ_{op} computed via eq. (20).

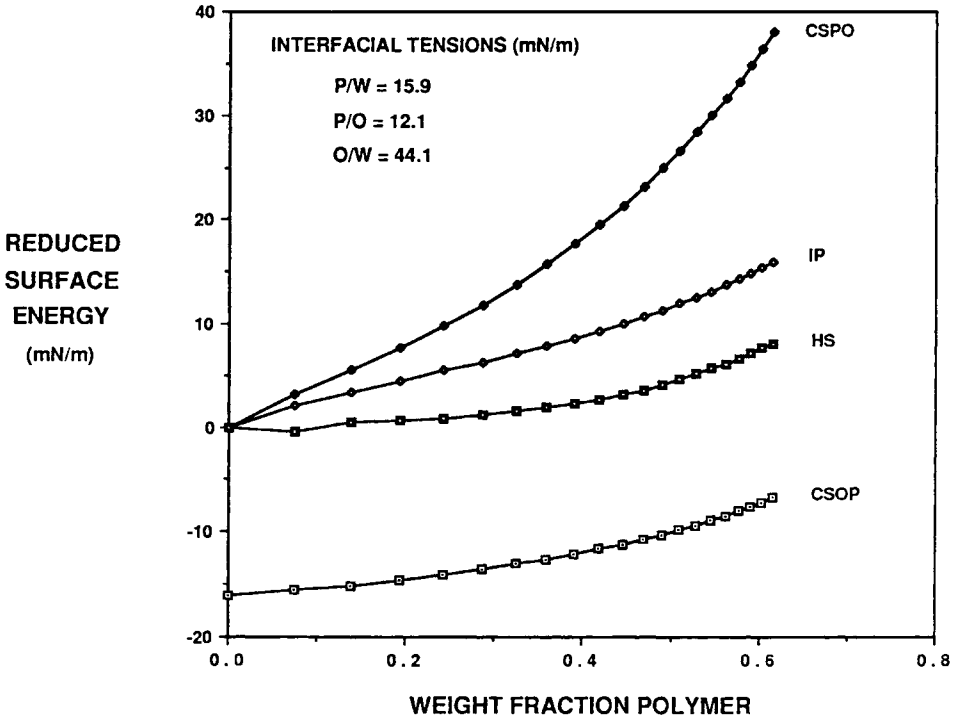

Fig. 4. Reduced surface energy ($\Delta\gamma$) curves for the PMMA/*n*-decane/MXP system.

Experiments were carried out in accordance with the procedures described earlier and the resulting morphologies can be compared to the predicted results noted above. Experiments utilizing the physical processing route (path A in Fig. 3) were carried out with both *n*-decane and mineral oil as the oil phase. Figure 6 shows the morphology of PMMA/*n*-decane particles resulting from an emulsion prepared with MXP as surfactant. This photomicrograph shows that the particles appear as spheres with the surface composed of PMMA (liquid oil at the surface has very different visual characteristics, as shown later). Although these particles were not sectioned to discern interior structure, the *n*-decane can easily be released from the particle by crushing it and thus it is likely that the morphology is of the core-shell type (CSOP). This is in accordance with the predictions resulting from Figure 4. By simply changing the type of surfactant from MXP to SLS the resulting morphology changes from that shown in Figure 6 to that of Figure 7. Here it is very apparent that the particles have taken a hemispherical arrangement, as predicted by the computations shown in Figure 5. In Figure 7 the smooth portion of the particle is *n*-decane and the PMMA surface displays the same lack of smoothness as shown in Figure 6. Such surface roughness is thought to be due to the Marangoni effect,[16] which relates surface depressions to the presence of interfacial tension gradients along the surface (see ref. 4 for a related discussion).

The second nonpolar oil used in this study was mineral oil. Its interfacial tension against water (with and without surfactant) is even greater than that of *n*-decane, as evidenced by the data shown in Table I. Figures showing the

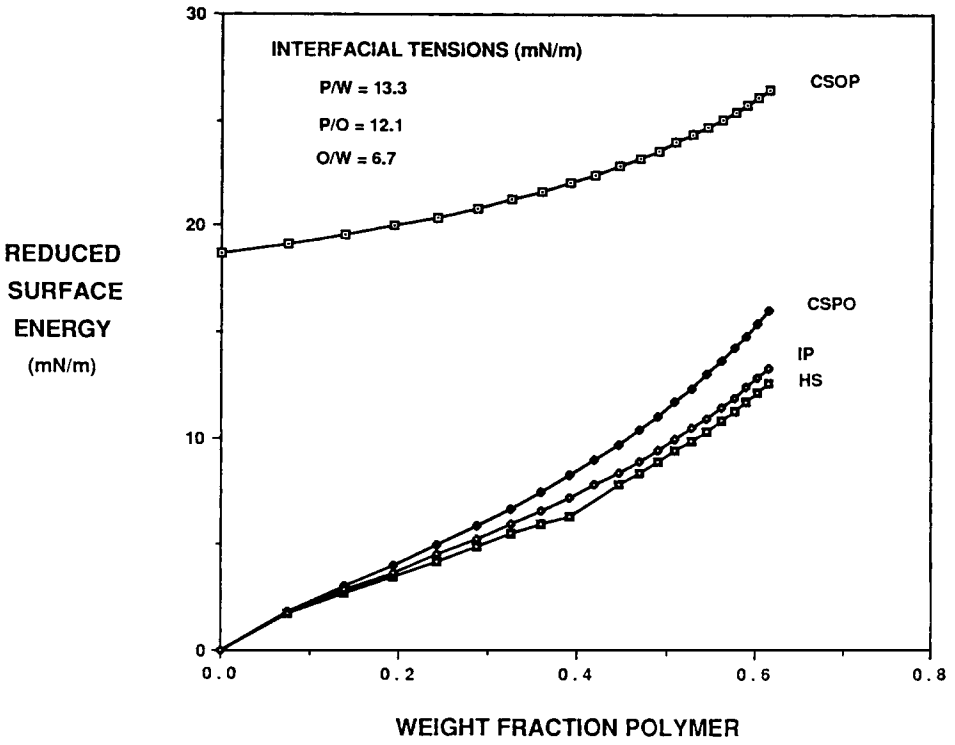

Fig. 5. Reduced surface energy ($\Delta\gamma$) curves for the PMMA/*n*-decane/SLS system.

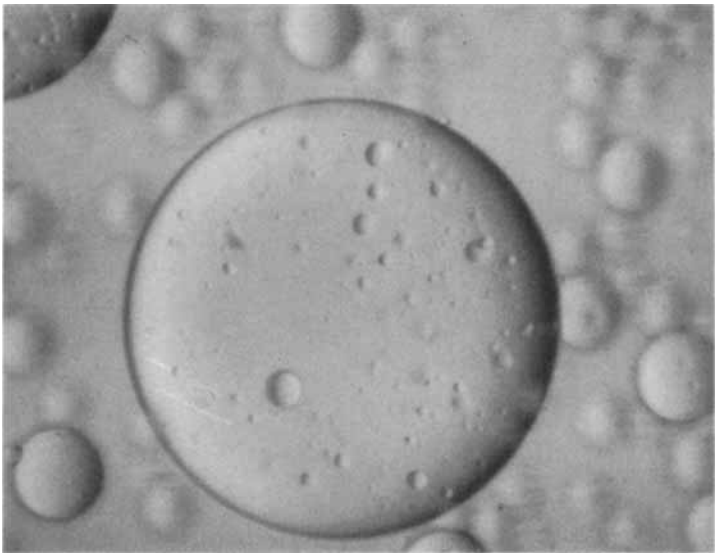

Fig. 6. Photomicrograph of particles after solvent removal for the PMMA/*n*-decane/MXP system. 200×.

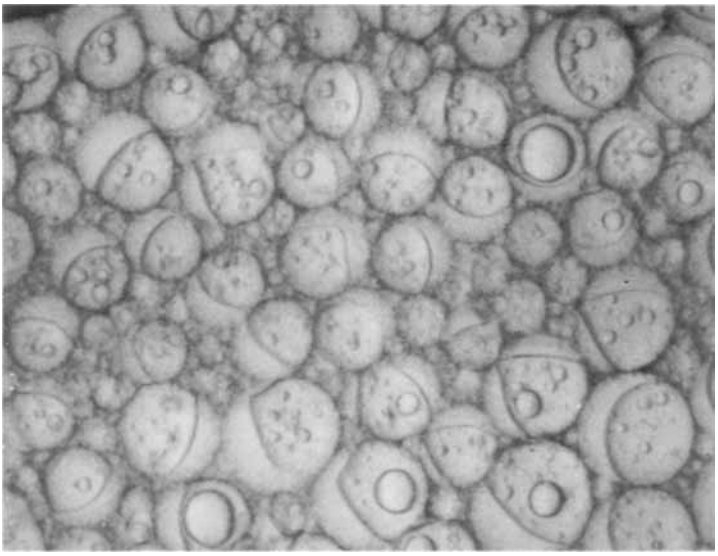

Fig. 7. Photomicrograph of particles after solvent removal for the PMMA/*n*-decane/SLS system. 200×.

reduced surface energies for this system have been omitted for brevity and because they show very similar results as the *n*-decane system. Experimental evidence for this PMMA/mineral oil system supports the predictions of core-shell (CSOP) morphology for the MXP surfactant (Fig. 8) and hemispherical morphology for the use of SLS (Fig. 9). An interesting observation has been

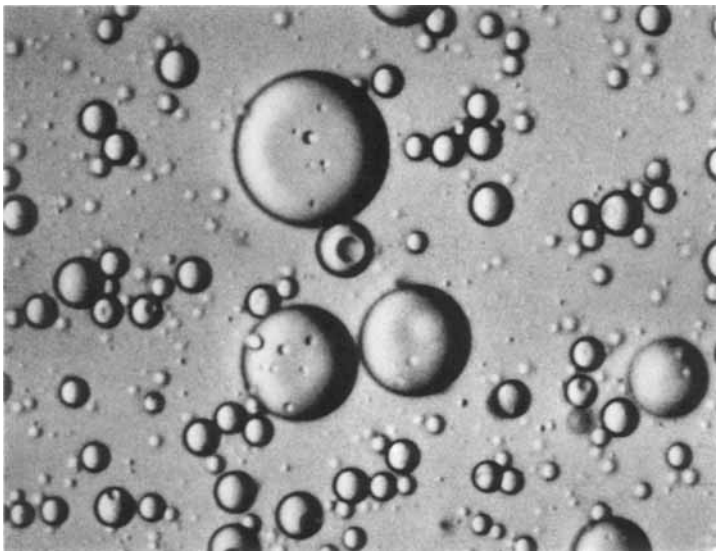

Fig. 8. Photomicrograph of particles after solvent removal for the PMMA/mineral oil/MXP system. 200×.

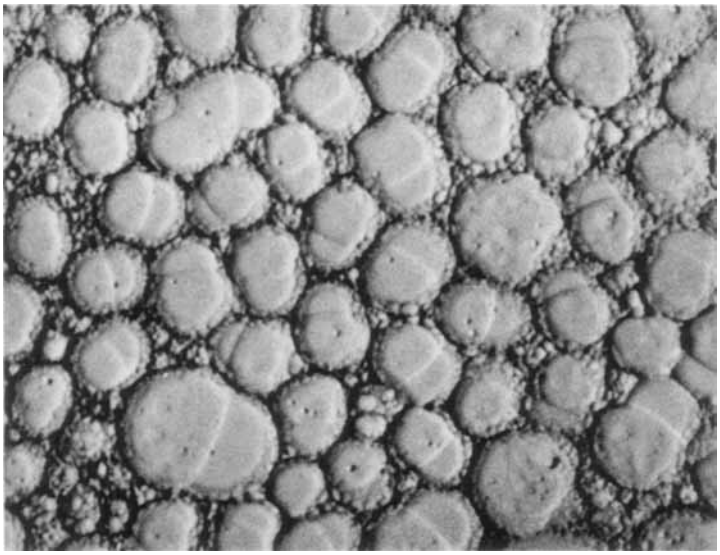

Fig. 9. Photomicrograph of particles after solvent removal for the PMMA/mineral oil/SLS system. 200×.

made for this PMMA/mineral oil/SLS system that shows several apparently different morphologies coexisting at one time within the same emulsion. Figure 10 shows several particles having multiple protrusions of oil on a central polymer phase. Such shapes are reminiscent of the sandwich structures[5] and "raspberry-like" particles[12] noted earlier as reported by other workers. Figure 10 corre-

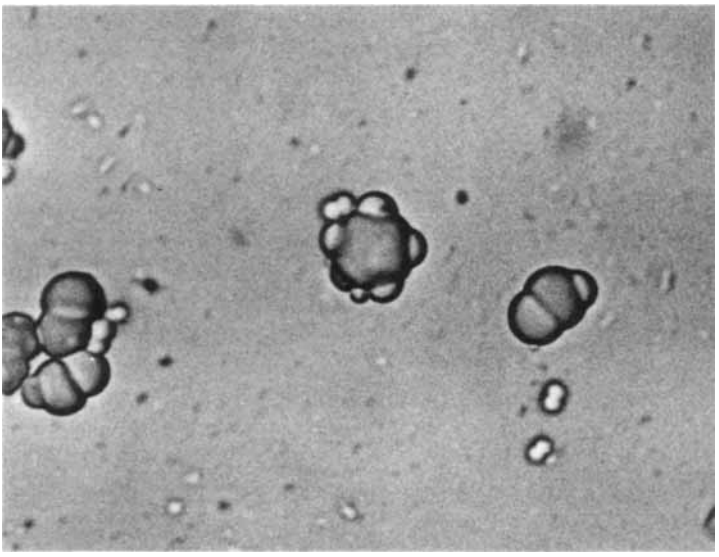

Fig. 10. Photomicrograph of particles after partial solvent removal for the PMMA/mineral oil/SLS system. 400×.

sponds to a sample in which not all of the solvent had been removed, and upon further removal of the solvent nearly all of the particles had been modified to complete hemispheres. Closer inspection of Figure 7 for the PMMA/*n*-decane/SLS system will also show that some of the particles appear to be nearly sandwich like while most have progressed to complete hemispheres. These results suggest that a number of apparently different morphologies previously reported may all be precursors of the hemispherical structure. Thermodynamics would certainly favor a completely phase-separated hemisphere over that of a sandwich or multiple protrusion arrangement. In a future report we will show the results of a videotape displaying the dynamic nature of the morphology development. This will show how the types of particles depicted in Figure 10 change to a final state of complete phase separation.

The results of the thermodynamic analyses reported in this paper are independent of the pathway chosen in Figure 3. Thus, we would expect similar results for the reactive processing path as we have found for the solvent removal process. Oil–water emulsions containing MMA monomer and a peroxide initiator were prepared with different surfactants and heated to effect *in situ* polymerization. The details have been reported elsewhere[4] but the inclusion of a few results are useful in the present discussion. Figure 11 shows the type of particles produced for the *in situ* polymerization of MMA in an *n*-decane/water emulsion stabilized with MXP. These particles are clearly core-shell (CSOP) and upon fracture reveal that all of the polymer is in the shell while the core is all oil.[4] A great variety of other surfactants were used in the same study and Figure 12 shows a typical result for the use of surfactants which, like SLS, greatly lower the oil–water interfacial tension. The particles shown in this figure are much like those shown in Figure 9 discussed earlier. It thus appears that whether or not polymerization reactions are involved in the

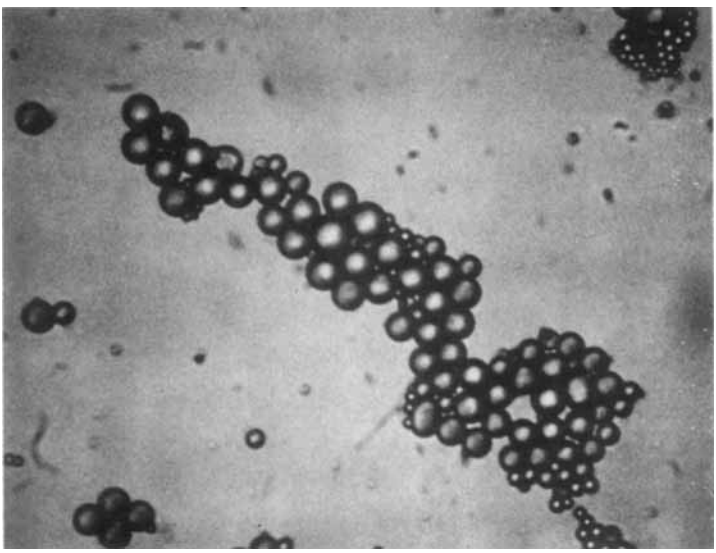

Fig. 11. Photomicrograph of particles formed via *in situ* polymerization of MMA within droplets of *n*-decane stabilized with MXP. 400×.

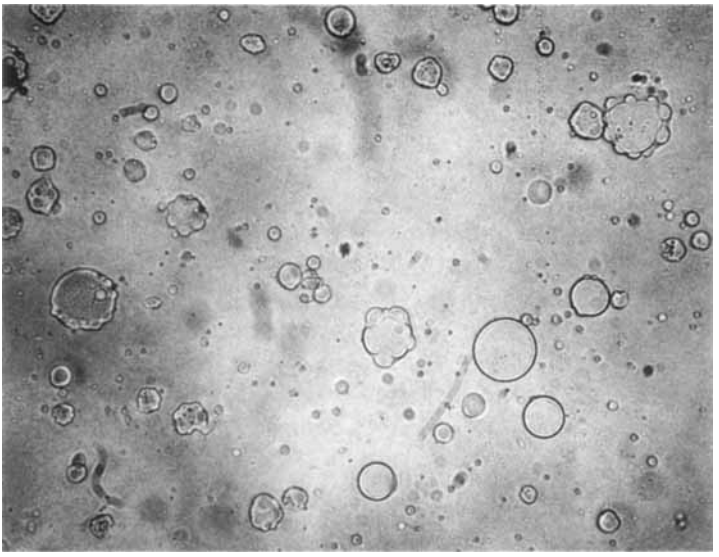

Fig. 12. Photomicrograph of particles formed via *in situ* polymerization of MMA within droplets of *n*-decane stabilized with a low surface tension surfactant (Ref. 4). 400×.

achievement of particle morphology, the thermodynamic analysis via surface free energies can provide correct predictions of particle morphology.

Before leaving this discussion it is worthwhile to return to the thermodynamic computations and Figures 4 and 5. As stated previously, all of the curves in Figure 4 are well separated and the most probable morphology is clearly distinguished. This is simply a result of the particular combination of γs involved. Because of such wide separation of the curves the precision of the value of γ_{op} obtained via eq. (20) is not a critical issue. However, as the values of the γs shift when one changes the surfactant or polymer(s) or oil, one may indeed be confronted by situations where the $\Delta\gamma$ curves are very close together. This places more importance upon the precision of calculated interfacial tensions, and upon experimental values as well. Figure 5 shows a situation in which it would appear that reasonably precise values of the γs would be required to make the correct choice between the hemisphere and the inverted core-shell morphologies, especially at low weight fractions of polymer. While it was first thought that the γ_{op} value predicted for the PMMA/*n*-decane interface was high for two organic materials, a review of measured γ_{op} values for different polymer pairs[17] showed that one may expect values from less than 1 mN/m to more than 10 mN/m. Large values (> 10) are apparently found for polymer pairs of widely different polarities [e.g., polyethylene–poly(vinyl acetate)]. Thus, considering that the pair of organics used in the present study are greatly different in polarity ($X^p = 0$ for *n*-decane and $X^p = 0.28$ for PMMA), it may be that the computed value of $\gamma_{op} = 12.1$ mN/m is a reasonably good estimate. In a future publication devoted to an extension of the present experimental system to a variety of different polymers and oils, the discussion of the required precision of the γ values will be rejoined.

CONCLUDING REMARKS

The central thrust of this report has been to emphasize the usefulness of simple thermodynamic considerations of surface free energies for the prediction of equilibrium morphologies of polymer particles prepared in emulsion form. Such an analysis highlights the relative importance of the various interfacial tensions and allows for the correct prediction of the role that the surfactant can play in affecting the equilibrium particle morphology. It can also aid in determining for which instances the value of γ_{op}, the interfacial tension between the two organic phases, will play an important role in morphology control. This might be especially useful when considering the impact of adding a small amount of block copolymer to the system or when debating the significance of graft copolymer formed *in situ* during a polymerization process.

Some of our results, such as those of Figure 10, strongly suggest that equilibrium morphologies are not always seen at the end of the experiment. This was not the case in the results of Torza and Mason[13] since they worked with incompatible pairs of low molecular weight compounds that diffuse readily. The replacement of one of these compounds with a high molecular weight polymer brings the issue of diffusive restrictions, i.e., polymer chain mobility, into consideration. We have found that it is entirely possible to achieve nonequilibrium morphologies, especially when the solvent is removed rapidly, even when one of the organic components is a low-viscosity liquid. We have designated such morphologies as "rate-limited morphologies" as contrasted to equilibrium morphologies and suggest that there may exist any number of states of phase separation (thus apparently different morphologies) depending upon the speed of the process (i.e., solvent evaporation or reaction kinetics). This is not a surprising result, especially for particles composed of two high molecular weight polymers, as would be found in synthetic latices. Although latex particles are commonly an order of magnitude smaller than those particles shown in Figures 4–12, the thermodynamic relations described in this paper are independent of particle size and should apply equally as well to latex particles.

The authors are grateful for partial financial support from the Swedish Board for Technical Development and the University of New Hampshire.

References

1. S. Krause, in *Polymer Blends, Volume I,* D. R. Paul and S. Newman, Eds., Academic Press, New York, 1978. pp. 15–113.

2. D. R. Paul and S. Newman, Eds., *Polymer Blends, Volume II,* Academic Press, New York, 1978.

3. J. Berg, D. Sundberg, and B. Kronberg, *Polym. Mater. Sci. Eng.,* **54,** 367 (1986).

4. J. Berg, D. Sundberg, and B. Kronberg, *J. Microencap.,* **6,** 327 (1989).

5. I. Cho and K.-W. Lee, *J. Appl. Polym. Sci.,* **30,** 1903 (1985).

6. D. I. Lee, *ACS Symp. Ser.,* **165,** 405 (1981).

7. T. I. Min et al., *J. Polym. Sci., Polym. Chem. Ed.,* **21,** 2845 (1983).

8. D. J. Hourston, R. Satgurunthan, and H. Varman, *J. Appl. Polym. Sci.,* **31,** 1955 (1986) and **33,** 215 (1987).

9. S. Muroi, H. Hashimoto, and K. Hosoi, *J. Polym. Sci., Polym. Chem. Ed.,* **22,** 1365 (1984).

10. D. I. Lee and T. Ishikawa, *J. Polym. Sci., Polym. Chem. Ed.,* **21,** 147 (1983).

11. D. R. Stutman, A. Klein, M. S. El-Aasser, and J. W. Vanderhoff, *Ind. Eng. Chem. Prod. Res. Dev.,* **24,** 404 (1985).

12. M. Okubo, Y. Katsuta, and T. Matsumoto, *J. Polym. Sci., Polym. Letters Ed.*, **20,** 45 (1982).

13. S. Torza and S. G. Mason, *J. Coll. Interf. Sci.*, **33,** 67 (1970).

14. J. L. Lando and H. T. Oakley, *J. Coll. Interf. Sci.*, **25,** 526 (1967).

15. S. Wu, *Polymer Interface and Adhesion,* Marcel Dekker, New York (1982).

16. J. C. Berg, In *Adv. Chem. Eng.*, **6,** 61–123 (1966), T. B. Drew and J. W. Hoopes, (Eds.), Academic Press, NY.

17. S. Wu, in *Polymer Blends, Volume I,* D. R. Paul and S. Newman, Eds., Academic Press, New York, p. 277 (1978).

APPENDIX

The simplified hemispherical morphology as depicted in Figure 2 does serve as a reasonably good approximation for the calculation of the surface free energy of the hemispherical morphology. However, for some systems the surface free energy calculated for the simplified hemispherical morphology and that for one of the other morphologies may be very close. In these instances a more accurate value for the hemispherical morphology is required. Figure A1 shows the actual shape of a two-phase, hemispherical particle, albeit with a flat interface between the two phases. Here the notation is

r_o = radius of spherical portion of original polymer phase
r_p = radius of spherical portion of secondary polymer phase
h_o = apparent penetration distance of original polymer phase into secondary polymer phase
h_p = apparent penetration distance of secondary polymer phase into original polymer phase.

The volume and interfacial areas of this particle geometry are readily found in standard mathematics handbooks and are written as

$$V_o = (4/3)\Pi r_o^3 - (\Pi/3)h_o^2(3r_o - h_o) \tag{A1}$$

$$V_p = (4/3)\Pi r_p^3 - (\Pi/3)h_p^2(3r_p - h_p) \tag{A2}$$

$$A_{ow} = 2\Pi(2r_0^2 - r_o h_o) \tag{A3}$$

$$A_{pw} = 2\Pi(2r_p^2 - r_p h_p) \tag{A4}$$

$$A_{op} = 2\Pi r_o h_o - \Pi h_o^2 = 2\Pi r_p h_p - \Pi h_p^2 \tag{A5}$$

Following the free energy analysis described earlier for the changes taking place in Figure 1, the free energy change for the actual hemispherical morphology is

$$(\Delta G)_{HS} = \gamma_{ow}[2\Pi(2r_o^2 - 2r_o h_o)] + \gamma_{pw}[2\Pi(2r_p^2 - r_p h_p)] + \gamma_{op}(2\Pi r_o h_o - \Pi h_o^2) - \gamma_{ow}[4\Pi(R_o')^2] \tag{A6}$$

The radius of the original particle, R_o', can be related to the parameters of the two phase particle in Figure A1 by equating the volumes of the original polymer in both particles. As such

$$R_o' = [r_o^3 - (h_o^2/4)(3r_o - h_o)]^{1/3} \tag{A7}$$

Normalizing eq. (A6) by the surface area of the original particle, $4\Pi(R_o')^2$, and using eq. (A7) yields

$$(\Delta\gamma)_{HS} = [\gamma_{ow}r_o(2r_o - h_o) + \gamma_{pw}r_p(2r_p - h_p) + \gamma_{op}h_o(r_o - h_o/2)]/\{2[r_o^3 - (h_o^2/4)(3r_o - h_o)]^{2/3}\} - \gamma_{ow} \tag{A8}$$

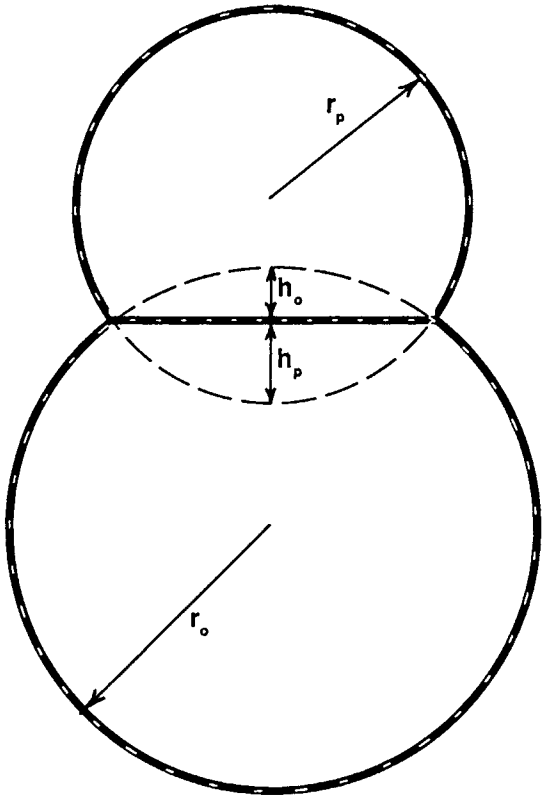

Fig. A1. Particle morphology for hemispherical analysis.

Taking the limit as ϕ_p goes to zero (which causes r_p, h_p, and h_o to be zero) yields $(\Delta\gamma)_{HS} = 0$, as of course it must.

To calculate $(\Delta\gamma)_{HS}$ via eq. (A8) at various volume fractions, ϕ_p, one must be able to relate r_o, h_o, r_p, and h_p to ϕ_p. There are any number of combinations of these rs and hs at a given ϕ_p which may conform to the geometric shape of Figure A1. However, only one of these combinations will be in the thermodynamic equilibrium state of lowest energy. That condition is determined by a trial and error process in which many different values of the rs and hs are used (noting that for a given ϕ_p there are restrictions on the values of r_p and h_p once r_o and h_o are chosen). That computation yielding the lowest interfacial energy at the chosen ϕ_p is taken as representing the proper combination of rs and hs. $(\Delta\gamma)_{HS}$ is then readily calculated via eq. (A8) and the process repeated at another value of ϕ_p.

Received April 14, 1989
Accepted September 26, 1989